BIOCHEMISTRY
including biophysical chemistry & molecular biology

ARTICLE

pubs.acs.org/biochemistry

# Mapping the Iron Binding Site(s) on the Small Tetraheme Cytochrome of *Shewanella oneidensis* MR-1

Yufeng Qian,[†] Catarina M. Paquete,[‡] Ricardo O. Louro,[‡] Daniel E. Ross,[§] Edward LaBelle,[§] Daniel R. Bond,[§] and Ming Tien*[,†]

[†]Department of Biochemistry and Molecular Biology, The Pennsylvania State University, University Park, Pennsylvania 16802, United States

[‡]Instituto de Tecnologia Química e Biológica, Av. da República (EAN), 2780-157 Oeiras, Portugal

[§]The BioTechnology Institute, University of Minnesota—Twin Cities, St. Paul, Minnesota 55108, United States

Supporting Information

**ABSTRACT:** In the model microbe *Shewanella oneidensis*, multi-heme proteins are utilized for respiratory metabolism where metals serve as the terminal electron acceptor. Among those is the periplasm-localized small tetraheme cytochrome (STC). STC has been extensively characterized structurally and electrochemically to which electron flow in and out of the protein has been modeled. However, until the present work, no kinetic studies have been performed to probe the route of electron flow or to determine the iron-binding site on STC. Using iron chelated by EDTA, NTA, or citrate, we have used chemical modification, site-directed mutagenesis along with isothermal titration calorimetry (ITC), and stopped-flow measurements to identify the iron binding site of STC. Chemical modifications of STC revealed that carboxyl groups on STC are involved in binding of EDTA−$Fe^{3+}$. Scanning mutagenesis was performed on Asp and Glu to probe the putative iron-binding site on STC. Two STC mutants (D21N; D80N) showed ∼70% decrease in observed electron transfer rate constant with EDTA−$Fe^{3+}$ from transient-state kinetic measurements. The impaired reactivity of STC (D80N/D21N) with EDTA−$Fe^{3+}$ was further confirmed by a significant decrease (>10-fold) in iron binding affinity.

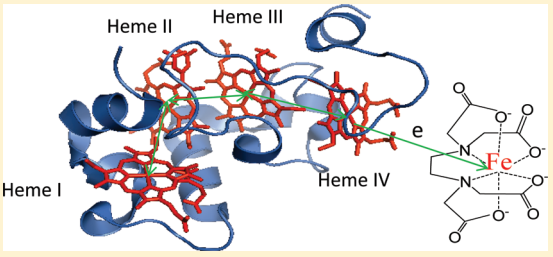


Respiratory metabolism evolved long before the use of molecular oxygen as a terminal electron acceptor (TEA). As such, microbes evolved the ability to utilize a wide range of TEAs.[1] Among the TEAs are insoluble metal oxides and soluble metal chelates.[2] The process of utilizing $Fe^{3+}$ as the TEA is referred to as dissimilatory iron reduction (DIR). Microbial DIR was first discovered with the facultative anaerobe *Shewanella*[3] which has since become a model organism for the study of DIR.[4] In addition to $Fe^{3+}$, *Shewanella* can also respire many other TEAs including $Mn^{3+}$, $Mn^{4+}$, and anthropomorphically generated $U^{6+}$ and $Tc^{6+}$.[5] Under anaerobic DIR growth conditions, *Shewanella* synthesizes a large number of multiheme *c*-type cytochromes that serve as a conduit for electron flow from the cytoplasmic membrane (CM) to the outer membrane (OM).[6−13] One such *c*-type cytochrome is the periplasm-localized small tetraheme cytochrome (STC). Two studies have demonstrated the importance of STC in DIR electron transfer. A knockout mutant of STC in *Shewanella frigidimarina* exhibits compromised growth using iron as the TEA but not fumarate.[13] In *S. oneidensis*, Coursolle et al.[14] have shown the importance of STC in electron transfer to soluble ferric chelates in knockout mutants of MtrA via a proposed MtrD-dependent manner.

STC has been extensively characterized structurally[15,16] and electrochemically.[17−22] NMR studies by both Harada et al.[17] and Fonseca et al.[20] proposed a directional electron transfer pathway within four hemes. More recently, Paquete et al.[21] applied the kinetic model to discriminate the contribution of each individual heme within each oxidation step of NTA−$Fe^{3+}$, and the modeling results led to the proposal that intermolecular electron transfer from the reduced STC to NTA−$Fe^{3+}$ occurs in the vicinity of heme I and heme IV. The dynamic simulation of STC interaction with hematite also showed electrons preferentially leave through heme I and heme IV.[23] However, no studies have been performed to test the validity of the models and also to determine the iron-binding site on STC. In the present study, we characterize the mechanism of electron transfer from reduced STC to three model ferric chelates: EDTA−$Fe^{3+}$, NTA−$Fe^{3+}$, and citrate−$Fe^{3+}$. We have used isothermal titration calorimetry (ITC) and transient-state kinetics to characterize the protein to metal interactions. Both methods demonstrated that STC binds the model soluble iron species at micromolar affinities, suggesting that STC is able to serve as the soluble ferric ion reductase. For the first time, we have identified Asp21 and Asp80 in the

**Received:** April 4, 2011
**Revised:** June 18, 2011
**Published:** June 19, 2011

vicinity of heme I and heme IV are involved in iron binding and reactivity.

## EXPERIMENTAL PROCEDURES

**Materials.** EDTA was purchased from EMD (EMD Chemicals). Spectra Multicolor Broad Range Protein Ladder was purchased from Fermentas (Fermentas Life Science). All other chemicals were purchased from Sigma/Aldrich Chemicals. The oligonucleotides for thrombin cleavage site introduction and primers for site-directed mutagenesis were purchased from Integrated DNA Technologies. The oligonucleotide sequences are shown in Table S1.

**Protein Expression and Purification.** STC was expressed as a his-tag fusion protein to facilitate purification after which the his tag was proteolytically removed. Plasmid *pET21a-stC* for overproduction of STC was constructed by ligating the *stC* DNA fragment into the NdeI-XhoI sites of *pET21a* (Novagen). STC was expressed in *Escherichia coli* BL21(DE3)/*pEC86* containing the *ccm*ABC-DEFGH (cytochrome *c* maturation) genes.[24] Cells of *E. coli* BL21(DE3) (*pET21-stC+PEC86*) strain were grown aerobically at 37 °C in Luria−Bertani medium (10 g/L tryptone, 10 g/L NaCl, 5 g/L yeast extract, pH adjusted with NaOH to 7.4) until the optical density reached 0.6. After another 10 h incubation with shaking at 30 °C, cells were harvested by centrifugation at 4000*g* at 4 °C for 10 min. The cell pellet was resuspended in 20 mM Tris-HCl, 20% sucrose, pH 8.0, (20 mL per gram of wet weight). The cells were treated with lysozyme (1 mg/mL), 1 mM EDTA, and 0.1 mM DTT and incubated at 37 °C for 1 h. The lysed cells were centrifuged at 20000*g* at 4 °C for 1 h. STC was purified from the supernatant using a 5 mL Ni-NTA column according to the manufacturer's protocol (Qiagen). Further purification was done through an Agilent fast protein liquid chromatograph at room temperature on a Mono-Q column; STC was eluted under a linear gradient of 0−250 mM NaCl over 10 column volumes. The purified STC was concentrated and the buffer exchanged into 20 mM Tris-HCl, pH 8.0, by ultrafiltration with a 10 kDa cutoff membrane (Pall Corp.).

**His-Tag Removal of STC.** To avoid possible competition between the His-tag and enzyme active site for iron binding, the His-tag was removed after Ni-column purification using an engineered C-terminal thrombin cleavage site.[25] The recombinant STC (10 $\mu$M) was dissolved in 20 mM Tris-Cl, pH 8.0, to which 0.1 Unit of thrombin was added. To remove any remaining His-tagged protein, the digested sample was passed through Ni-NTA column in 20 mM Tris-HCl, pH 8.0, 50 mM NaCl. The nonbound fraction contained the cleaved protein which was further purified over a Mono-Q column to remove thrombin.

**Ferric Complexes Preparation.** The molar ratio EDTA−$Fe^{3+}$ was prepared as 1:1 (and also 1.5:1 yielding identical results), with NTA−$Fe^{3+}$ and citrate−$Fe^{3+}$ prepared as 2.5:1 and 2:1, respectively. Equilibrium speciation calculations[26] showed that at such preparations the predominant Fe(III) species in the EDTA−$Fe^{3+}$ system is EDTA−$Fe^{3+}$ (85%), while the Fe(III) species in NTA−$Fe^{3+}$ and citrate−$Fe^{3+}$ system is $Fe^{3+}$−(NTA)-(OH) (99%) and $Fe^{3+}$−$(citrate)_2$ (69%), respectively.

**Isothermal Titration Calorimetry (ITC).** ITC measurements were carried out at 25 °C on the Nano-ITC II Instrument (TA Instruments). Prior to analysis, STC was dialyzed against 20 mM Tris-HCl buffer, pH 8.0, 50 mM NaCl. The titrants (ferric chelates) were dissolved in the spent dialysis buffer. Prior to measurements, all solutions were degassed under vacuum with stirring. The solution in the sample cell was stirred at 300 rpm to ensure rapid mixing and heat equilibrium. In a typical titration, 5−8 $\mu$L of titrant was injected into a solution of 50 $\mu$M STC over a period of 10 s with an adequate interval (2−5 min) between injections to allow complete equilibrium. Anaerobic measurements were performed under a $N_2$ atmosphere. Ferrous ion solutions were prepared under anaerobic conditions and thoroughly deoxygenated before each experiment was carried out. Titrations were carried out until no further heat change was observed following addition of titrants. To correct for dilution and mixing effects, the control titration, which consisted of the same titration solution, but with buffer in the sample cell, was subtracted from each experiment, accounting for the heat of dilution.

A minimum of two titrations were carried out for each measurement, and the reported experimental values are the average of individual best-fit values, determined with one-set binding model in the Nano Analyze software provided by TA Instruments. ITC results are presented by showing baseline-adjusted experimental titration data (heat flow versus time) on the top and peak-integrated background-subtracted concentration-normalized molar heat flow per aliquot versus the injection time on the bottom.

**Transient State Kinetic Analysis of STC.** STC was reduced enzymatically using xanthine oxidase as described before[27] with the following modifications: STC (1 $\mu$M) in 20 mM Tris-HCl, pH 8.0, was incubated with xanthine (1.5 mM), xanthine oxidase (0.02 U/mL), and benzyl viologen (2 $\mu$M) anaerobically ($N_2$). The extent of the reduction process was monitored by the increase in 550 nm absorbance. The reaction of reduced STC (1 $\mu$M) with soluble ferric iron species was monitored in an Applied Photosystems (Surrey, United Kingdom) SX.18MV stopped-flow spectrophotometer with a 1 cm path-length cell. The reaction with ferric complexes was monitored at 419 nm associated with ferroheme oxidation. The overall observed electron transfer rate constant ($k_{obs}$) was extracted by fitting the trace using the single-exponential decay model of Sigma Plot 10.0 (Systat Software Inc.).

**Analysis of Kinetic Traces from Experiments with EDTA−$Fe^{3+}$.** The data obtained for the oxidation of STC by EDTA−$Fe^{3+}$ were fitted to a kinetic model.[21] This model can be applied when there is fast intramolecular electron exchange and slow intermolecular electron exchange, allowing the protein to be under thermodynamic control between each of the sequential electron transfer steps. Under these conditions the complex kinetic scheme that describes the four-center protein collapses to a simple kinetic system of four consecutive one-electron transfer steps represented by four macroscopic rate constants, $k_I$−$k_{IV}$. These macroscopic rate constants are set by the weighted average of the microscopic rate constants of all the microsteps that participate in that macroscopic step. And each of these microscopic rate constants is parsed into a contribution of the driving force of the particular step using an exponential term derived from Marcus theory[21] and a reference rate constant that is intrinsic to each heme that is related to structural factors. The fit of the model to the kinetic data was performed for EDTA−$Fe^{3+}$ as previously reported for the oxidizing agent NTA−$Fe^{3+}$ using the Nelder−Mead algorithm implemented in MATLAB.[28]

**Chemical Modification of STC with TNBS and EDC−HCl.** To chemically modify lysine residues, STC (50 $\mu$M) in 1% (w/v) sodium bicarbonate buffer pH 9.0 was incubated in the absence or presence of varying concentrations of 2,4,6-trinitrobenzenesulfonic

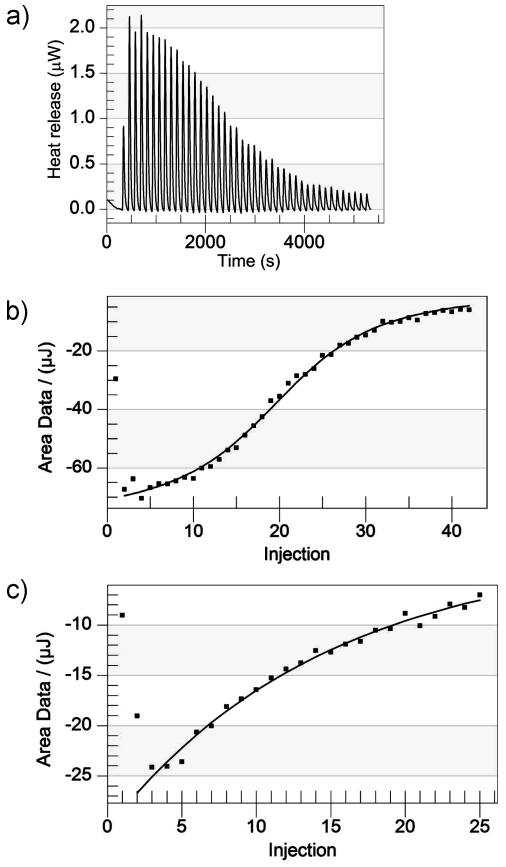


**Figure 1.** ITC measurement of exothermic binding of STC to EDTA−$Fe^{3+}$ or EDTA−$Fe^{2+}$ at pH 8.0 (20 mM Tris-HCl, 100 mM NaCl) and 25 °C. (a) Raw data obtained for continuous injections of 5 μL of 0.64 mM EDTA−$Fe^{3+}$ to 40 μM STC. The area of each peak represents the total heat evolved upon addition of a single aliquot of EDTA−$Fe^{3+}$. (b) Titration plot derived from the integrated heats of binding of (a), corrected for heat of dilution. (c) ITC measurement of exothermic binding of STC to EDTA−$Fe^{2+}$ at pH 8.0 (20 mM Tris-HCl, 100 mM NaCl) and 25 °C anaerobically in an $N_2$ atmosphere. The black line represents the nonlinear best fit to the data assuming a single-set binding model.

acid (TNBS) at 37 °C for 1 h. The reaction was quenched by addition of 1 M sodium acetate, pH 5.2. The STC protein was subsequently separated from the reaction mixtures on a Sephadex G-25 gel filtration column with buffer exchanged into 20 mM Tris-HCl at pH 8.0.

For carboxyl group modification, STC (50 μM) in MES buffer at pH 5.5 was incubated in the presence of 3 mM 1-ethyl-3-[3-(dimethylamino)propyl]carbodiimide hydrochloride (EDC−HCl) and 10 mM ethylenediamine at room temperature in the dark for 1 h. The reaction was stopped by adding 1 M Tris-HCl, pH 8.0, and then passed through Sephadex G-25 gel filtration column as described earlier.

**Site-Directed Mutagenesis of STC.** Plasmid *pET21a-stC* was used as a template in the QuickChange site-directed mutagenesis (Strategene) procedure according to manufacturer's instructions. Forward and reverse mutagenic primers used to create the point mutations are summarized in Table S1. The sequence shown in bold represent bases introduced to obtain the desired mutation. The desired mutation was subsequently confirmed by DNA sequencing.

**Table 1. ITC Analyses of STC Binding with Ferric and Ferrous Complexes**[a]

| STC protein | $K_d$ (μM) | $\Delta H°$ (kJ/mol) | $\Delta G°$[b] (kJ/mol) | $n$ |
|---|---|---|---|---|
| EDTA−$Fe^{3+}$ | 7.2 ± 1.2 | −23.2 ± 4.2 | −29.3 ± 0.3 | 1.9 ± 0.3 |
| NTA−$Fe^{3+}$ | 11.3 ± 1.1 | −31.1 ± 4.5 | −28.2 ± 0.2 | 1.8 ± 0.1 |
| citrate−$Fe^{3+}$ | 100 ± 2.3 | −5.2 ± 1.9 | −22.8 ± 0.1 | 2.2 ± 0.1 |
| EDTA−$Fe^{2+}$ | 92 ± 22.1 | −24.9 ± 2.8 | −23.0 ± 0.3 | 0.3 ± 0.2 |
| NTA−$Fe^{2+}$ | 37 ± 8.2 | −23.4 ± 8.2 | −25.2 ± 0.5 | 0.6 ± 0.1 |

[a] All ferrous complexes binding experiments were performed anaerobically to avoid ferrous oxidation. [b] Calculated from $\Delta G = -RT \ln K$.

**Protein Film Voltammetry of STC and STC(D21N).** Protein film voltammetry (PFV) experiments were performed using a VMP3 potentiostat (Bio-Logic, Knoxville, TN). Baseline measurements were collected for freshly polished glassy carbon electrodes at 4 °C in a pH 7 degassed mixed buffer solution of 5 mM HEPES, 5 mM MES, 100 mM NaCl, 10 μM neomycin, as adapted from Firer-Sherwood and co-workers.[19] Data were collected at 25 °C at 10 and 100 mV/s. Data were analyzed and processed using SOAS.[29]

## RESULTS

**Purification of Recombinant His-Tag Free STC.** Because metal binding will be characterized in this study, it was necessary to remove the His tag from the recombinant STC. A thrombin protease recognition site was engineered into the recombinant protein. The sequencing of Leu-Val-Pro-Arg-Gly-Ser was inserted at the C-terminal end of *stC* gene upstream of the His-tag encoding sequence. Complete removal of the His tag (1.23 kDa) was confirmed by SDS−PAGE. Proteins were visualized by Coomassie dye staining and by heme-linked peroxidase staining as described previously.[30] The results showed that STC was purified to greater than 95% homogeneity and that the his-tag was removed from the recombinant protein (Figure S1A,B).

**Isothermal Titration Calorimetry (ITC) Studies on Metal Binding.** The interactions between STC and model soluble ferric complexes including EDTA−$Fe^{3+}$, NTA−$Fe^{3+}$, and citrate−$Fe^{3+}$ were studied by ITC. STC was dialyzed against 20 mM Tris-HCl, pH 8.0, 50 mM NaCl. The ITC measurements show that STC has greater affinity for EDTA−$Fe^{3+}$ with $K_d$ (7.2 ± 1.2 μM) and NTA−$Fe^{3+}$ (11.3 ± 1.1 μM) compared to citrate−$Fe^{3+}$ (100 μM). Figure 1a shows representative ITC data from the titration of 40 μM STC with EDTA−$Fe^{3+}$ at 25 °C. The data were integrated and fitted with one-set binding model to determine the best-fit value for the experimental dissociation constant ($K_d$), stoichiometry ($n$), and enthalpy change ($\Delta H$) associated with the binding. The average values from each of the ferric complexes from three independent experiments are shown in Table 1. As a control, we also used ITC to determine the binding affinity of STC with just the chelator, without ferric ion. Little or no binding was detected with either NTA (Figure S2) or citrate.

**Binding of Ferrous Complexes to STC.** ITC was also used to determine the binding affinity of STC to ferrous complexes. EDTA−$Fe^{2+}$ and NTA−$Fe^{2+}$ were examined under $N_2$-purged anaerobic conditions. Table 1 summarizes the best-fit values for the dissociation constant ($K_d$) and enthalpy change ($\Delta H$) associated with the binding. Our results show that STC binds ferric complexes more tightly than ferrous complexes. For EDTA−$Fe^{3+}$, the $K_d$ is 7.2 μM, while the $K_d$ of EDTA−$Fe^{2+}$

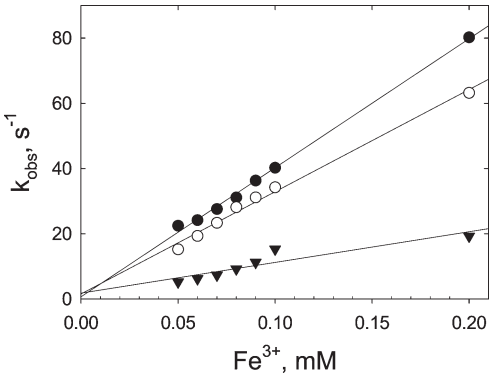


**Figure 2.** Reaction of reduced STC (1 $\mu$M) with ferric iron chelates. Observed rate constants ($k_{obs}$) are plotted against various concentrations of EDTA−$Fe^{3+}$ (●), NTA−$Fe^{3+}$ (○), and citrate−$Fe^{3+}$ (▼).

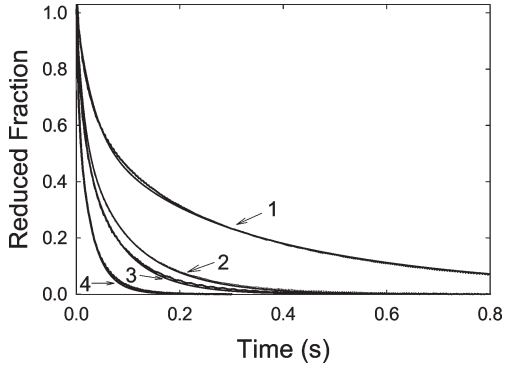


**Figure 3.** Kinetics of oxidation of STC by EDTA−$Fe^{3+}$. Black dots are the kinetic data, and black lines are the fit of the kinetic model to the data. The concentrations of EDTA−$Fe^{3+}$ were 20 $\mu$M (1), 60 $\mu$M (2), 80 $\mu$M (3), 100 $\mu$M (4), and 1 $\mu$M of STC for pH 8.0 after mixing, respectively.

is 92 $\mu$M (Figure 1c). It is interesting to note that all ferric complexes (EDTA−$Fe^{3+}$, NTA−$Fe^{3+}$, and citrate−$Fe^{3+}$) show the similar stoichiometry of around 2, indicating that STC may contain two distinct noninteracting iron binding sites exhibiting similar intrinsic binding affinities (Table 1). In contrast, all ferrous ligands have possessed a binding stoichiometry less than 1 (Table 1). This again is in agreement with the relative weaker ferrous binding affinity of STC which does not permit saturation during the titration experiment.

**Reaction of Ferric Complexes by Reduced STC.** Rate constants for the reduction of ferric complexes by reduced STC were measured with a stopped-flow spectrophotometer in an anaerobic chamber. STC was reduced enzymatically by incubation with xanthine, xanthine oxidase, and the redox mediator benzyl viologen. Very low amounts of xanthine oxidase were added such that complete reduction of STC would take place over 3−4 h. This ensured that absorbance changes observed during the time course of STC oxidation, as monitored in the stopped flow over milliseconds, was not complicated by rereduction processes. The reactions were monitored by following the decrease at 419 or 552 nm absorbance associated with the oxidation of ferroSTC to ferricSTC. Reaction of ferroSTC with ferric chelates resulted in a single-exponential decrease in the absorbance. Consistent with ITC results, STC reacts to EDTA−$Fe^{3+}$ or NTA−$Fe^{3+}$ much faster than citrate−$Fe^{3+}$ (Figure 2). Observed electron transfer rate constants

**Table 2. Reference Rate Constants for Each Heme of STC during the Oxidation with EDTA−$Fe^{3+}$ at 25 °C for pH 8.0[a]**

| | $k_i^0$ ($\times 10^7$ $M^{-1}$ $s^{-1}$) | | | |
|---|---|---|---|---|
| | heme I | heme II | heme III | heme IV |
| EDTA−$Fe^{3+}$ | 46.8 (0.7) | 0.0 (1.0) | 0.0 (0.4) | 0.9 (0.6) |

[a] Standard errors are given in parentheses considering an experimental uncertainty of 5% of the total amplitude of the optical signal in the kinetic traces.

**Table 3. Fraction of Electrons That Leave STC in Each One-Electron Oxidation Step with EDTA−$Fe^{3+}$**

| | heme I | heme II | heme III | heme IV |
|---|---|---|---|---|
| step 1[a] | 0.91 | 0 | 0 | 0.09 |
| step 2 | 0.83 | 0 | 0 | 0.17 |
| step 3 | 0.45 | 0 | 0 | 0.55 |
| step 4 | 0.27 | 0 | 0 | 0.73 |
| total | 2.36 | 0 | 0 | 1.64 |

[a] In previous work,[21] the redox steps were numbered starting from the oxidized state whereas in this table they are numbered starting from the reduced state of STC.

($k_{obs}$) are plotted as a function of different concentrations of $Fe^{3+}$ substrate. The slope of each linear fitted line can approximately represent the forward rate constant ($k_1$) based on the reaction model described before.[26,27] The calculated $k_1$ of ferroSTC reacting with EDTA−$Fe^{3+}$ is 3.9 $\times$ $10^5$ $M^{-1}$ $s^{-1}$.

**Kinetic Analysis To Discriminate Contribution of Each Heme.** The stopped flow experiments with EDTA−$Fe^{3+}$ were fitted with a kinetic model that uses the previously determined thermodynamic parameters for the hemes of STC.[21] This analysis permitted discrimination of the kinetic contribution of each heme to the overall rate of electron transfer. The fits for the oxidation of fully reduced STC with EDTA−$Fe^{3+}$ are shown in Figure 3. A possible explanation for the small deviation between the calculated and experimental curves which is more noticeable for the data obtained with 20 $\mu$M EDTA−$Fe^{3+}$ is the speciation of EDTA−$Fe^{3+}$ which has a minor form under the conditions of the experiment. The fit of the kinetic traces with the kinetic model yielded the reference rate constants for the four different hemes and are shown in Table 2. The reference rate constants obtained from the fit can be used, in turn, with the driving force associated with each transition and the population fraction of each microscopic state reported in the literature,[20] to determine the contribution of each heme to each of the sequential macroscopic oxidation steps (Table 3).

The model indicates that oxidation of fully reduced STC is dominated by heme I for the first and for the second step. Heme I also has the most negative reduction potential and thus possesses the strongest driving force for oxidation by EDTA−$Fe^{3+}$. For the third electron, heme IV plays a more significant role in electron transfer, and for the fourth and last oxidation step, heme IV is the predominant exit point.

**Chemical Modification of STC.** The modeling studies suggested the importance of heme I and heme IV in STC oxidation. The validity of the model was investigated using chemical modification studies and also site-directed mutagenesis. We first used chemical modification of STC to narrow down the list of

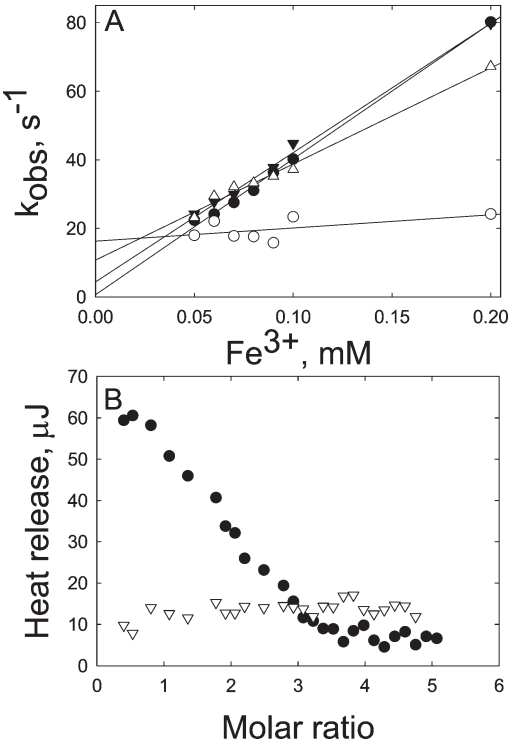


**Figure 4.** (A) Rate constants ($k_{obs}$) of 1 $\mu$M STC (●), STC (lysine residues modified, ▼), STC (carboxyl groups modified, ○) STC (EDTA−$Fe^{3+}$ protected, △) reacting with EDTA−$Fe^{3+}$ as a function of various concentrations of EDTA−$Fe^{3+}$. (B) ITC determinations of binding affinity of EDTA−$Fe^{3+}$ binding to STC (●) and STC (carboxyl groups modified, ○).

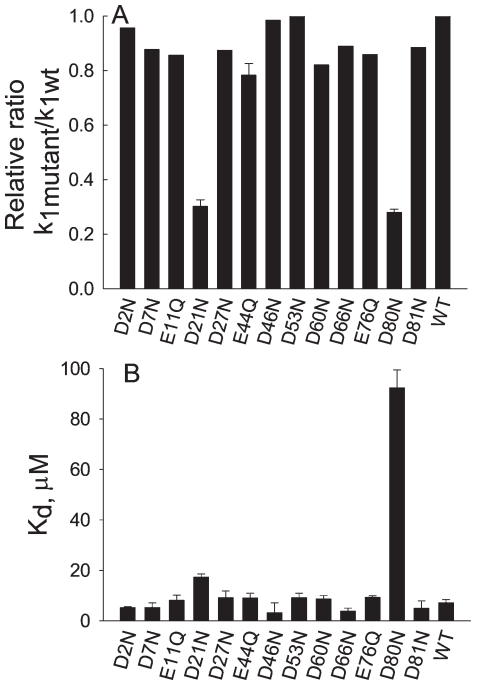


**Figure 5.** Comparison of reactivity and binding affinity of STC purified from each mutant binding and reacting to EDTA−$Fe^{3+}$: (A) relative ratio of $k_1$ of mutant ferroSTC reacting with EDTA−$Fe^{3+}$ compared to wild type; (B) comparison of $K_d$ measured by ITC.

possible amino acids involved in iron-chelate binding. We used TNBS, an amine group modifier,[31] and EDC−HCl, a modifier of the carboxyl group.[32] TNBS modification had little if any effect on the reactivity of ferroSTC with the ferric chelates (Figure 4A). Likewise, the binding isotherm of STC with chelated $Fe^{3+}$ was not effected (data not shown). In contrast, the modification of carboxyl group resulted in a large decrease in the electron transfer rate between ferroSTC and EDTA−$Fe^{3+}$ (Figure 4A). ITC measurements were also performed, and in corroboration with the stopped-flow results, little to no binding was observed between carboxyl-group modified STC and EDTA−$Fe^{3+}$ (Figure 4B). These results are consistent with either Asp or Glu residues being involved in $Fe^{3+}$ binding. NMR spectrometry of carboxylic acid-modified STC shows that the paramagnetically shifted signals of the hemes which include heme methyls and propionate α-protons are unaffected by the treatment (data not shown).

To investigate whether the iron binding site can be protected by the (iron) substrate, 50 $\mu$M STC was incubated with EDC−HCl but also with EDTA−$Fe^{3+}$ (500 $\mu$M). After modification, the reactivity of STC with EDTA−$Fe^{3+}$ was studied by stopped-flow kinetics. In contrast to the nonprotected EDC−HCl-modified protein, the rate constants were only slightly decreased ($k_1 = 2.8 \times 10^5\ M^{-1}\ s^{-1}$ compared to $3.9 \times 10^5\ M^{-1}\ s^{-1}$). This is consistent with protection of STC by preincubation with EDTA−$Fe^{3+}$ in EDC−HCl modification (Figure 4A). Thus, our results show that carboxyl groups and not lysine groups are involved in binding to EDTA−$Fe^{3+}$.

**Site-Directed Mutagenesis.** To identify the carboxyl group involved in iron binding, we systematically mutated all of the Asp and Glu residues in STC. Wild type and 15 STC mutants were expressed in *E. coli* BL21(DE3) (*pET21a-stC* + *pEC86*) and purified as described before (data not shown). The binding constants and rate constants were obtained through kinetic characterization and by ITC as previously performed for wild type STC (Figure 5A,B). Two mutants, one at $Asp^{80}$ and one at $Asp^{21}$, exhibited a dramatic decrease in reactivity of EDTA−$Fe^{3+}$ as assessed by stopped-flow measurements. ITC results supported the data from the stopped-flow experiments; STC (D80N) showed more than 10 times decrease in binding affinity with EDTA−$Fe^{3+}$. Similar ITC characterization of D21N was not as straightforward. We are not clear why STC (D21N) shows no significant difference in binding to EDTA−$Fe^{3+}$ while it reacts at a slower rate with the substrate. $Asp^{80}$ and $Asp^{21}$ are both solvent exposed and close to the porphyrin ring. $Asp^{80}$ is localized within 8 Å to heme IV, and $Asp^{21}$ is within 7 Å of heme I. This close proximity would permit electron transfer between the heme and the docked iron within a subsecond time scale.[33] Mutation of $Asp^{80}$ to Gly or Ala yielded no significant difference from mutation to Asn (data not shown), indicating the carboxylate of $Asp^{80}$ is essential for iron binding which cannot be restored by the carboxamide of $Asn^{80}$. We also investigated the role of amino acids close to $Asp^{80}$ in iron binding. Double mutations of D80N/D81N, D80N/E78Q, and D80N/D21N did not further impede the electron transfer rate.

**Redox Potential of D21N.** D21N differs from D80N in that the decrease in the rate of electron transfer is not proportionately observed in the binding constant as measured by ITC. As such, D21N was further characterized. Our ongoing NMR characterization of the D21N shows that these factors are identical for the WT and the mutant which suggests the structure of the WT is maintained in D21N. PMV was then performed to investigate the effect of the mutation on the redox potential of STC (D21N).

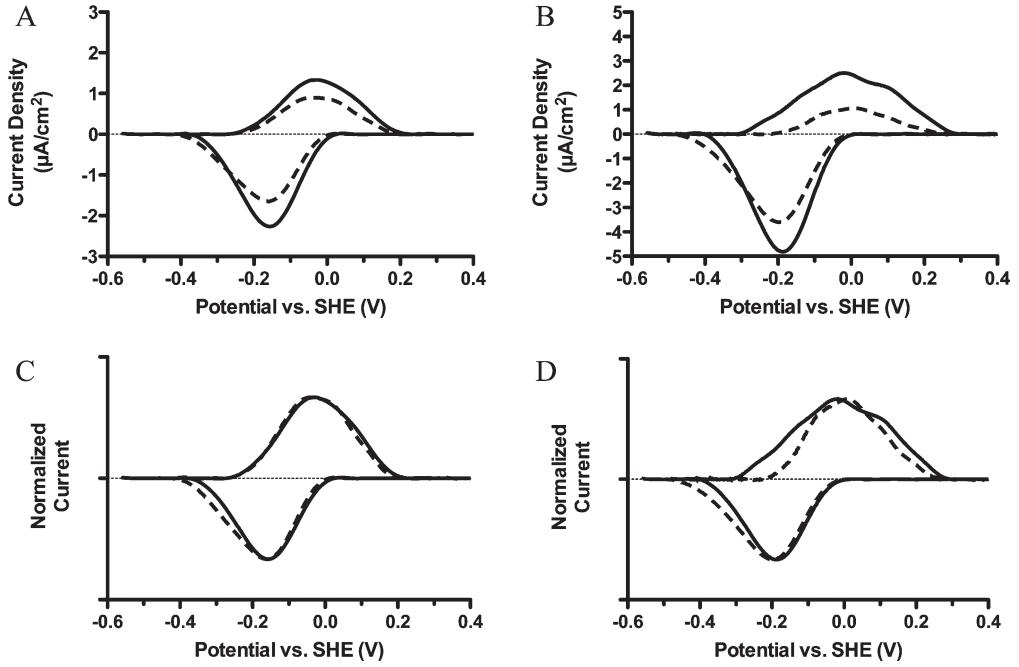


**Figure 6.** Protein film voltammetry of STC (WT) and STC (D21N). Baseline-subtracted representative data of WT (solid) and D21N (dashed) absorbed onto glassy carbon at 25 °C, pH 7.0, with 100 mM NaCl and 10 mM neomycin. Current density (A, B) and peak current normalized (C, D) data. Scan rates are 10 (A, C) and 100 mV/s (B, D).

The purified protein was adsorbed onto a glassy carbon electrode and placed in an anaerobic, temperature-controlled, three-electrode glass cell. Cyclic sweeps of 10 and 100 mV/s from −560 to 240 mV vs (standard hydrogen electrode) SHE were performed at 4, 10, and 25 °C. At 25 °C, films of WT and D21N had midpoint potentials of −93 and −98 mV vs SHE, respectively. At a scan rate to 100 mV/s, WT and D21N maintained within 10 mV of their midpoint potential (Figure 6). This suggests that the overall redox potential of STC is not significantly affected by the mutation of D21 to N21 on STC. The decrease in ET transfer rate is perhaps attributed to the absence of one electron exit site.

## DISCUSSION

The genome of *S. oneidensis* encodes 42 predicted, *c*-type cytochromes of which many contain multiple hemes.[34] Many of these hemeproteins are known to participate in anaerobic respiratory electron transfer not only in the CM but also in the periplasm and the OM.[35,36] The protein studied here, STC, is periplasm localized and, of the multiheme proteins synthesized by *Shewanella*, is perhaps the most well characterized. While the role of STC in respiratory metabolism has yet to be clearly defined, our results here show that STC has the kinetic constants consistent with it acting as a terminal ferric reductase. The rate constants and the binding constants with three different iron forms indicate that STC is an excellent ferric reductase. While STC may be involved in ferric ion reduction in the periplasm, our studies here only use this reaction to probe the route of electron transfer out of reduced STC. While much has been done to model this process,[17,20,21,23] there has been very little experimental evidence to support any of the models.

Modeling the electron transfer process has been possible due to the structural information along with the thermodynamic parameters of heme reduction.[15,17,20] On the basis of the intra- and inter-heme distances, Leys et al.[15] proposed that electron transfer can occur between any heme of one STC molecule to any heme of another STC. Thus, each heme is proposed to be able to accept or donate electrons independent of any other heme moieties. This then enables rapid intramolecular electron transfer and also increases the chance of intermolecular electron transfer between STC and its redox partner.[15] However, Harada et al.[17] proposed a mechanism of directional electron transfer. These workers determined the redox potential of the four hemes of STC using NMR at high pH. They also examined the heme geometry in respect to accessibility of the electron acceptor. On the basis of these considerations, these workers proposed that the exit point for electrons is heme IV. This oxidation is then followed by rapid electron movement between the four hemes. Fonseca et al.[20] also showed evidence for directional electron transfer in STC from *S. oneidensis*. A detailed thermodynamic characterization of the protein was performed using NMR and visible spectroscopy. STC was titrated with various redox mediators to obtain samples of varied reduction states. The NMR signal of the heme methyl groups was then used to monitor the redox state of each of the four hemes. Their results show that heme I is mostly oxidized throughout all of the partially reduced states. Thus, Fonseca et al.[20] proposed that donors feed electrons through heme I and then are redistributed to the other hemes according to their reduction potentials in the sequence of III, IV, II, and then I. For electron transfer out of STC, heme III has the lowest accessibility, and on the basis of the similarity of structure to flavocytochrome *c*3,[37] Fonseca et al.[20] suggested heme IV to be the electron exit point. Another study from the same lab also indicated directional electron transfer for STC.[21] Using reduction potential values for each heme as well as the heme−heme interaction energies, Paquete et al.[21] determined the redox state of each heme as it undergoes the successive stages of reduction (initially not commenting on the route of electron

entry or exit). They found that heme III is reduced in the one-electron-reduced state (stage 1, S1) since it has the highest reduction potential. The second, third, and final electron resides in heme IV, heme II, and then heme I. Using such a model, they were able to model the kinetics of STC oxidation by NTA−$Fe^{3+}$.

While the above studies have determined the redox state of each heme through each stage of the reduction process and have modeled the electron transfer process involving each heme, no studies to date have substantiated the model and have identified the iron binding site for STC. The present study was performed to investigate the mechanism of this process in respect to the route of electron transfer within the hemes of STC and to locate the iron-binding site. Our ITC results with three soluble iron forms showed the following binding affinities EDTA−$Fe^{3+}$ > NTA−$Fe^{3+}$ > citrate−$Fe^{3+}$. Surprisingly, recognition and binding occurs with the chelate iron forms and not the free chelate. No binding is detected between STC and either NTA or citrate alone (in absence of iron). Alkylating agents for both basic and acidic amino acids were first used to determine the location of the iron binding site(s). Amino acid-alkylating agent TNBS had no effect on iron binding, whereas the carboxyl-group-modifying agent EDC−HCl decreased the rate of STC reduction of ferric chelates. These observations are consistent with molecular dynamic calculation results of STC binding to hematite where Kerisit et al.[23] found 67% of the hydrogen bonds formed between STC and solid iron surfaces are composed of Asp and Glu residues.[23]

Further experiments using site-directed mutagenesis identified the carboxyl-bearing residues D21 and D80 in proximity to heme I and IV, respectively. Both residues are within 10 Å of the porphyrin ring plane of each heme,[15] and both mutations resulted in a significant decrease in the rate of electron transfer to chelated iron (Figure 5A,B). A change in $K_d$ for the mutants was also observed; however, for the D21N mutant, the change (increase) in $K_d$ was not as great as that observed for the rate of electron transfer. We have no apparent explanation for this small discrepancy. Furthermore, fits of the ITC results from both STC(D21N) and STC(D80N) yield a stoichiometry of approximately one binding site compared to two for wild-type STC. The multiple iron binding sites have been observed in other ferric reductases and iron transport proteins.[38,39] As an example, the structure of the ferric reductase from *Archaeoglobus fulgibus* has revealed two potential iron binding sites for reduction.[38]

To the best of our knowledge, our study described here is the first study to identify the iron binding site on STC. In conclusion, our results in this study are in agreement with unidirectional electron transfer within the tetraheme STC. While the protein partners of STC have yet to be determined, our results indicate that the protein has specific binding sites for soluble ferric complexes. These binding sites are capable of distinguishing between the ferric and ferrous complex. In addition, binding occurs only when the ferric ion is bound to the chelate. The location of the chelated iron bindings sites are in agreement with modeling studies performed by Paquete et al.[21] On-going studies in our lab seek to determine the protein binding partners of STC with the overall goal of elucidating the overall electron transfer pathway.

## ■ ASSOCIATED CONTENT

**Ⓢ Supporting Information.** Primers used for the site-direct mutagenesis, experimental data about purification of STC, ITC measurement of NTA binding to STC, and spectroscopic characterization of mutants. This material is available free of charge via the Internet at http://pubs.acs.org.

## ■ AUTHOR INFORMATION

### Corresponding Author

*E-mail: mxt3@psu.edu; phone: +8148631165; fax: +8148637024.

### Funding Sources

This work was supported by the NSF Environmental Molecular Sciences Institute program (CHE-0431328) through the Penn State Center for environmental Kinetics Analysis and by DOE grant ER64399 0013153.

## ■ ACKNOWLEDGMENT

We thank Dr. Marty Bollinger (Penn State University) for the use of stopped flow. Some of the ITC experiments were performed in the laboratory of Dr. Jeffrey Catchmark (Penn State University).

## ■ ABBREVIATIONS

STC, small tetraheme cytochrome; EDTA, ethylenediaminetetraacetic acid; NTA, nitrilotriacetic acid; TNBS, 2,4,6-trinitrobenzenesulfonic acid; EDC−HCl, , 1-ethyl-3-[3-(dimethylamino)propyl]-carbodiimide hydrochloride.

## ■ REFERENCES

(1) Madigan, M. T., Martinko, J. M., and Parker, J. (2000) *Brock Biology of Microorganisms*, Prentice Hall, Upper Saddle River, NJ.

(2) Weber, K. A., Achenbach, L. A., and Coates, J. D. (2006) Microorganisms pumping iron: anaerobic microbial iron oxidation and reduction. *Nat. Rev. Microbiol. 4*, 752–764.

(3) Myers, C. R., and Nealson, K. H. (1988) Bacterial manganese reduction and growth with manganese oxide as the sole electron acceptor. *Science 240*, 1319–1321.

(4) Lovley, D. R. (1991) Dissimilatory Fe(III) and Mn(IV) reduction. *Microbiol. Rev. 55*, 259–287.

(5) Fredrickson, J. K., Zachara, J. M., Kennedy, D. W., Duff, M. C., Gorby, Y. A., Li, S. M. W., and Krupka, K. M. (2000) Reduction of U(VI) in goethite (alpha-FeOOH) suspensions by a dissimilatory metal-reducing bacterium. *Geochim. Cosmochim. Acta 64*, 3085–3098.

(6) Beliaev, A. S., Saffarini, D. A., McLaughlin, J. L., and Hunnicutt, D. (2001) MtrC, an outer membrane decahaem c cytochrome required for metal reduction in *Shewanella putrefaciens* MR-1. *Mol. Microbiol. 39*, 722–730.

(7) Schwalb, C., Chapman, S. K., and Reid, G. A. (2003) The tetraheme cytochrome CymA is required for anaerobic respiration with dimethyl sulfoxide and nitrite in Shewanella oneidensis. *Biochemistry 42*, 9491–9497.

(8) Pitts, K. E., Dobbin, P. S., Reyes-Ramirez, F., Thomson, A. J., Richardson, D. J., and Seward, H. E. (2003) Characterization of the *Shewanella oneidensis* MR-1 decaheme cytochrome MtrA. *J. Biol. Chem. 278*, 27758–27765.

(9) Myers, C. R., and Myers, J. M. (1992) Localization of Cytochromes to the Outer-Membrane of Anaerobically Grown Shewanella-Putrefaciens Mr-1. *J. Bacteriol. 174*, 3429–3438.

(10) Myers, J. M., and Myers, C. R. (2001) Role for outer membrane cytochromes OmcA and OmcB of *Shewanella putrefaciens* MR-1 in reduction of manganese dioxide. *Appl. Environ. Microbiol. 67*, 260–269.

(11) Hartshorne, R. S., Reardon, C. L., Ross, D., Nuester, J., Clarke, T. A., Gates, A. J., Mills, P. C., Fredrickson, J. K., Zachara, J. M., Shi, L., Beliaev, A. S., Marshall, M. J., Tien, M., Brantley, S., Butt, J. N., and Richardson, D. J. (2010) Characterization of an electron conduit

between bacteria and the extracellular environment. *Proc. Natl. Acad. Sci. U. S. A. 106*, 22169–22174.

(12) Tsapin, A. I., Vandenberghe, I., Nealson, K. H., Scott, J. H., Meyer, T. E., Cusanovich, M. A., Harada, E., Kaizu, T., Akutsu, H., Leys, D., and Van Beeumen, J. J. (2001) Identification of a small tetraheme cytochrome c and a flavocytochrome c as two of the principal soluble cytochromes c in *Shewanella oneidensis* strain MR1. *Appl. Environ. Microbiol. 67*, 3236–3244.

(13) Gordon, E. H. J., Pike, A. D., Hill, A. E., Cuthbertson, P. M., Chapman, S. K., and Reid, G. A. (2000) Identification and characterization of a novel cytochrome c(3) from *Shewanella frigidimarina* that is involved in Fe(III) respiration. *Biochem. J. 349*, 153–158.

(14) Coursolle, D., and Gralnick, J. A. (2010) Modularity of the Mtr respiratory pathway of Shewanella oneidensis strain MR-1. *Mol. Microbiol. 77*, 995–1008.

(15) Leys, D., Meyer, T. E., Tsapin, A. S., Nealson, K. H., Cusanovich, M. A., and Van Beeumen, J. J. (2002) Crystal structures at atomic resolution reveal the novel concept of "electron-harvesting" as a role for the small tetraheme cytochrome c. *J. Biol. Chem. 277*, 35703–35711.

(16) Paixao, V. B., Salgueiro, C. A., Brennan, L., Reid, G. A., Chapman, S. K., and Turner, D. L. (2008) The solution structure of a tetraheme cytochrome from Shewanella frigidimarina reveals a novel family structural motif. *Biochemistry 47*, 11973–11980.

(17) Harada, E., Kumagai, J., Ozawa, K., Imabayashi, S., Tsapin, A. S., Nealson, K. H., Meyer, T. E., Cusanovich, M. A., and Akutsu, H. (2002) A directional electron transfer regulator based on heme-chain architecture in the small tetraheme cytochrome c from Shewanella oneidensis. *FEBS. Lett. 532*, 333–337.

(18) Akutsu, H., and Takayama, Y. (2007) Functional roles of the heme architecture and its environment in tetraheme cytochrome c. *Acc. Chem. Res. 40*, 171–178.

(19) Firer-Sherwood, M., Pulcu, G., and Elliott, S. (2008) Electrochemical interrogations of the Mtr cytochromes from Shewanella: opening a potential window. *J. Biol. Inorg. Chem. 13*, 849–854.

(20) Fonseca, B. M., Saraiva, I. H., Paquete, C. M., Soares, C. M., Pacheco, I., Salgueiro, C. A., and Louro, R. O. (2009) The tetraheme cytochrome from Shewanella oneidensis MR-1 shows thermodynamic bias for functional specificity of the hemes. *J. Biol. Inorg. Chem. 14*, 375–385.

(21) Paquete, C. M., Saraiva, I. H., Calcada, E., and Louro, R. O. (2010) Molecular Basis for Directional Electron Transfer. *J. Biol. Chem. 285*, 10370–10375.

(22) Paquete, C. M., and Louro, R. O. (2010) Molecular details of multielectron transfer: the case of multiheme cytochromes from metal respiring organisms. *Dalton Trans. 39*, 4259–4266.

(23) Kerisit, S., Rosso, K. M., Dupuis, M., and Valiev, M. (2007) Molecular computational investigation of electron-transfer kinetics across cytochrome-iron oxide interfaces. *J. Phys. Chem. C 111*, 11363–11375.

(24) Thony-Meyer, L., Fischer, F., Kunzler, P., Ritz, D., and Hennecke, H. (1995) *Escherichia coli* genes required for cytochrome c maturation. *J. Bacteriol. 177*, 4321–4326.

(25) Chang, J. Y. (1986) The Structures and Proteolytic Specificities of Autolysed Human Thrombin. *Biochem. J. 240*, 797–802.

(26) Wang, Z., Liu, C., Wang, X., Marshall, M. J., Zachara, J. M., Rosso, K. M., Dupuis, M., Fredrickson, J. K., Heald, S., and Shi, L. (2008) Kinetics of reduction of Fe(III) complexes by outer membrane cytochromes MtrC and OmcA of *Shewanella oneidensis* MR-1. *Appl. Environ. Microbiol. 74*, 6746–6755.

(27) Ross, D. E., Brantley, S. L., and Tien, M. (2009) Kinetic Characterization of OmcA and MtrC, Terminal Reductases Involved in Respiratory Electron Transfer for Dissimilatory Iron Reduction in Shewanella oneidensis MR-1. *Appl. Environ. Microbiol. 75*, 5218–5226.

(28) Lagarias, J. C., Reeds, J. A., Wright, M. H., and Wright, P. E. (1998) Convergence Properties of the Nelder--Mead Simplex Method in Low Dimensions. *SIAM J. Optim. 9*, 112–147.

(29) Fourmond, V., Hoke, K., Heering, H. A., Baffert, C., Leroux, F., Bertrand, P., and Leger, C. (2009) SOAS: A free program to analyze electrochemical data and other one-dimensional signals. *Bioelectrochemistry 76*, 141–147.

(30) Thomas, P. E., Ryan, D., and Levin, W. (1976) Improved Staining Procedure for Detection of Peroxidase-Activity of Cytochrome-P-450 on Sodium Dodecyl-Sulfate Polyacrylamide Gels. *Anal. Biochem. 75*, 168–176.

(31) Jagtap, S., and Rao, M. (2006) Conformation and microenvironment of the active site of a low molecular weight 1,4-beta-D-glucan glucanohydrolase from an alkalothermophilic Thermomonospora sp.: Involvement of lysine and cysteine residues. *Biochem. Biophys. Res. Commun. 347*, 428–432.

(32) Schlick, T. L., Ding, Z. B., Kovacs, E. W., and Francis, M. B. (2005) Dual-surface modification of the tobacco mosaic virus. *J. Am. Chem. Soc. 127*, 3718–3723.

(33) Page, C. C., Chen, X., Moser, C. C., and Dutton, L. P. (1998) Natural engineering principles of electron tunnelling in biological oxidation-reduction. *Nature 402*, 47–52.

(34) Heidelberg, J. F., Paulsen, I. T., Nelson, K. E., Gaidos, E. J., Nelson, W. C., Read, T. D., Eisen, J. A., Seshadri, R., Ward, N., Methe, B., Clayton, R. A., Meyer, T., Tsapin, A., Scott, J., Beanan, M., Brinkac, L., Daugherty, S., DeBoy, R. T., Dodson, R. J., Durkin, A. S., Haft, D. H., Kolonay, J. F., Madupu, R., Peterson, J. D., Umayam, L. A., White, O., Wolf, A. M., Vamathevan, J., Weidman, J., Impraim, M., Lee, K., Berry, K., Lee, C., Mueller, J., Khouri, H., Gill, J., Utterback, T. R., McDonald, L. A., Feldblyum, T. V., Smith, H. O., Venter, J. C., Nealson, K. H., and Fraser, C. M. (2002) Genome sequence of the dissimilatory metal ion-reducing bacterium Shewanella oneidensis. *Nature Biotechnol. 20*, 1118–1123.

(35) Shi, L., Squier, T. C., Zachara, J. M., and Fredrickson, J. K. (2007) Respiration of metal (hydr)oxides by Shewanella and Geobacter: a key role for multihaem c-type cytochromes. *Mol. Microbiol. 65*, 12–20.

(36) Clarke, T. A., Holley, T., Hartshorne, R. S., Fredrickson, J. K., Zachara, J. M., Shi, L., and Richardson, D. J. (2008) The role of multihaem cytochromes in the respiration of nitrite in Escherichia coli and Fe(III) in *Shewanella oneidensis*. *Biochem. Soc. Trans. 036*, 1005–1010.

(37) Leys, D., Tsapin, A. S., Nealson, K. H., Meyer, T. E., Cusanovich, M. A., and Van Beeumen, J. J. (1999) Structure and mechanism of the flavocytochrome c fumarate reductase of Shewanella putrefaciens MR-1. *Nat. Struct. Biol. 6*, 1113–1117.

(38) Chiu, H. J., Johnson, E., Schroder, I., and Rees, D. C. (2001) Crystal structures of a novel ferric reductase from the hyperthermophilic archaeon Archaeoglobus fulgidus and its complex with NADP(+). *Structure 9*, 311–319.

(39) Huang, J., Dizin, E., and Cowan, J. A. (2008) Mapping iron binding sites on human frataxin: implications for cluster assembly on the ISUFe-S cluster scaffold protein. *J. Biol. Inorg. Chem. 13*, 825–836.